Materials Science Forum
ISSN: 1662-9752, Vol. 1157, pp 33-41
doi:10.4028/p-BJgP7H

Submitted: 2024-09-21
Revised: 2025-05-31
Accepted: 2025-05-31
Online: 2025-09-05

Formation of Alternating Epilayers of 4H-SiC and 3C-SiC by Simultaneous Lateral Epitaxy

H. Nagasawa[1,a*], M. Abe[2,b], T. Tanno[2,c], M. Musya[2,d], M. Sakuraba[2,3,e], S. Sato[2,3,f], Y. Watanabe[4,g] and M. Suemitsu[1,h]

[1]CUSIC Inc. 2-2-10 Chuo, Aoba, Sendai, Miyagi, 980-0021 Japan

[2]RIEC, Tohoku Univ., 2-1-1 Katahira, Aoba, Sendai 980-8577, Japan

[3]Grad. Sch. Eng., Tohoku Univ.,6-6 Aramaki Aza Aoba, Aoba, Sendai 980-8579, Japan

[4]Seiko Epson Corp., 281 Fujimi, Fujimi-machi, Suwa-gun, Nagano 399-0293, Japan

[a]nags@cusic.co.jp, [b]maho.abe.a8@tohoku.ac.jp, [c]takenori.tanno.a7@tohoku.ac.jp, [d]michimasa.musya.a4@tohoku.ac.jp, [e]sakuraba.masao@myad.jp, [f]shigeo@tohoku.ac.jp, [g]Watanabe.Yukimune@exc.epson.co.jp, [h]suemitsu@cusic.co.jp

Keywords: 3C-SiC, 4H-SiC, Heteroepitaxy, EBSD, TEM, Coherent Interface, Scanning Probe Microscopy, 2DEG, 2DHG

Abstract. To generate both two-dimensional electron gas (2DEG) and two-dimensional hole gas (2DHG) at will in SiC polytype heterojunctions, simultaneous lateral epitaxy (SLE) method has been extended to form epilayers of alternating stacks of 4H- and 3C-SiC, which includes the first formation of single-domain 4H-SiC(0001) on 3C-SiC(111). The process starts with a spontaneous generation of mononuclear 3C-SiC on the atomically flat wide terrace on 4H-SiC, which expands parallel to the basal plane to form a single-domain 3C-SiC layer having the coherent interface with the underlying 4H-SiC layer. Step-controlled epitaxy is then applied using the adjacent 4H-SiC steps to grow an alternative 4H-SiC layer on top of the 3C-SiC surface, forming another coherent interface. The crystal structure, the interface structure, and the carrier distribution of these stacked epilayers were analyzed. Finally, it is demonstrated that 2DEG occurs at the coherent interface between the 3C-SiC(111) Si- and 4H-SiC$(000\bar{1})$ C-faces and 2DHG at the 3C-SiC$(\bar{1}\bar{1}\bar{1})$ C- and 4H-SiC(0001) Si-faces.

Introduction

Semiconductor devices based on polytype heterojunctions are an attractive application of SiC. Recently, a high electron mobility transistor (HEMT) utilizing the two-dimensional electron gas (2DEG) generated at the 3C/4H-SiC heterojunction has been demonstrated by Sazawa et al. [1, 2]. To grow the desired 3C-SiC epilayer on the C-face of 4H-SiC substrate suitable for 2DEG, they precisely tuned the off-orientation and the off-angle at proper values. This epitaxial growth technique, however, is not compatible with the wide-spread step-controlled epitaxy, a standard epitaxial growth in the SiC industry. Another limitation of their method is that only 2DEG forms on the 4H-SiC C-face and it is necessary to change the substrate to the Si-face to realize two-dimensional hole gas (2DHG). To overcome these limitations, we have extended our original growth method of simultaneous lateral epitaxy (SLE) [3, 4] to be able to form epilayers of alternating stacks of 4H-SiC and 3C-SiC. The conventional SLE is implemented by step-controlled epitaxy on groove patterned off-axis 4H-SiC(0001) Si-face. The heterojunction obtained by this SLE, however, consists of a coherent interface between 4H-SiC(0001) Si-face and 3C-SiC$(\bar{1}\bar{1}\bar{1})$ C-face, which generates 2DHG [5]. To generate 2DEG using SLE, the interface must consist of the 4H-SiC$(000\bar{1})$ C-face and 3C-SiC(111) Si-face [6]. To obtain both 2DEG and 2DHG at will, we have extended SLE to be able to form alternating stacks of epilayers of 4H-SiC and 3C-SiC.

To form single-domain 3C-SiC on 4H-SiC, 3C-SiC mononuclear (η_C) must be generated spontaneously on the atomically flat wide terrace (WT) in the basal plane of 4H-SiC, which is a necessary condition for eliminating the double-positioning boundary (DPB). When the width of the narrowest part of the WT exceeds a critical value for spontaneous nucleation (w_c), η_C generates near

the center of the WT [3]. Contrary to the 3C-SiC nucleation on the 4H-SiC surface, the 4H-SiC nucleation on the 3C-SiC surface is practically impossible even if the 3C-SiC surface is atomically flat. This is because the stacking sequence of 4H-SiC is not uniquely determined on 3C-SiC. The 4H-SiC layer on 3C-SiC should be formed by a similar manner of step-controlled epitaxy, with lateral expansion of existing 4H-SiC steps.

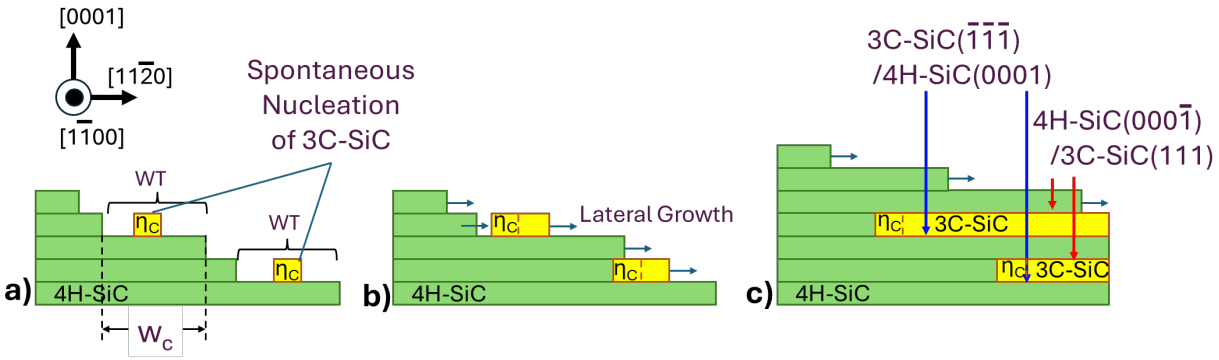

Fig. 1. Schematic section of alternating epitaxial growth of 4H- and 3C-SiC: a) 3C-SiC nuclei (η_C) are generated on atomically flat wide terrace (WT) and shift in the [0001] direction; b) Then, the 3C-SiC layers originating from η_C and the surrounding 4H-SiC layers expand in the [11$\bar{2}$0] direction (downstream); c) Finally, a 4H-SiC layer is inserted between each 3C-SiC layer.

In this study, the nucleation sites of η_C are arranged on misoriented 4H-SiC substrate so that the stacking sequence originally contained in the 4H-SiC substrate propagates laterally on 3C-SiC layers as schematically shown in Fig. 1 a). It should be noted that each η_C is shifted to a relative in the [0001] direction. Then, as shown in Fig. 1 b), the 3C-SiC layer originating from η_C and surrounding the 4H-SiC layer expand in the [11$\bar{2}$0] direction (downstream) by step-controlled epitaxy. Finally, a 4H-SiC layer can be inserted between each 3C-SiC layer (Fig.1 c). The above method produces two types of coherent interfaces simultaneously. One is a boundary between 3C-SiC($\bar{1}\bar{1}\bar{1}$) C- and 4H-SiC(0001) Si-faces. The other is a boundary between 3C-SiC(111) Si- and 4H-SiC(000$\bar{1}$) C-faces. The crystal structure and carrier distribution of the SiC epilayer including each one of the coherent interfaces are analyzed in detail.

Experimental

A 4H-SiC wafer with a surface with Si-face tilted by 4 degrees in the [11$\bar{2}$0] direction relative to the (0001) plane was used as a substrate for SLE. Before the epitaxial growth, grooves of 0.8 μm-depth were formed on the substrate surface by photolithography and dry etching techniques. All groove edges were deflected away from the [$\bar{1}$100] direction forming vertices (τ as the initial letter) in the [$\bar{1}\bar{1}$20] direction, and this creates isolated zigzag-shaped plateaus (PL as the initial letter), as schematically shown in Fig. 2. The η_C is generated near each τ on the PL, which is the most [0001] oriented portion on the PL, in a similar manner to the method disclosed by Larkin et al. [7]. Each PL and τ are arranged alternately in the [11$\bar{2}$0] direction. For example, PL_1 locates on the [$\bar{1}\bar{1}$20] direction side (upstream) of τ_2, and τ_3 locates on the [11$\bar{2}$0] direction side (downstream) of PL_2. In the epitaxial growth process described later, as shown in Fig. 1 b), the edge of PL_1 grows laterally in the [11$\bar{2}$0] direction, and it is possible to form a stacked layer of PL_1 on the 3C-SiC layer originating τ_2. The spacing of adjacent τ in the [$\bar{1}$100] direction (P), the width of groove (S), the displacement of τ in the [$\bar{1}\bar{1}$20] direction (Z), and the width of PL (W) are varied independently to observe their effect on the stacked structure of SiC epilayer. In this study, we focus on the different behavior of the epitaxial growth in two characteristic areas, each of which contains grooves with varying dimensions. The dimensions of the three grooves in the first area (area-1) are Z=10 μm, S=8 μm, P=40 μm, W=150 μm, while those in the second area (area-2) are Z=20 μm, S=4 μm, P=40 μm, and W=150 μm.

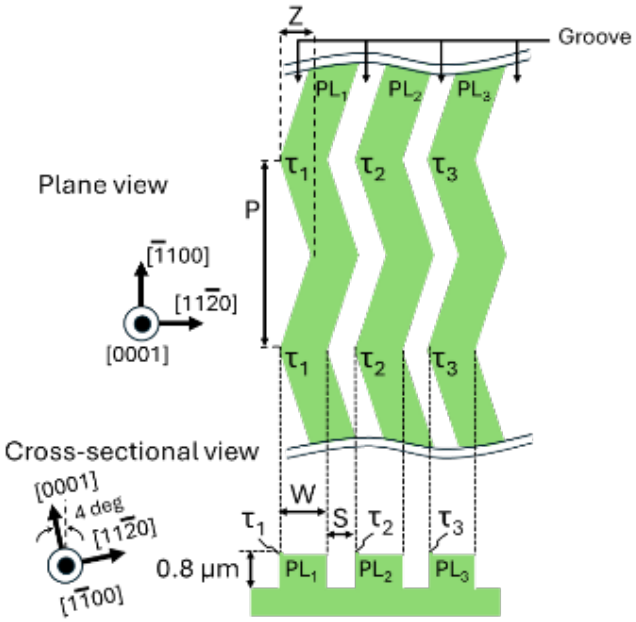

Fig. 2. Configuration of grooves formed on 4H-SiC substrate: All groove edges were deflected away from the $[1\bar{1}00]$ direction forming vertices (τ) in the $[\bar{1}\bar{1}20]$ direction, which creates isolated zigzag plateaus (PL) separated by grooves. The spacing of adjacent τ in the $[1\bar{1}00]$ direction (P), the width of groove (S), the displacement of τ in the $[\bar{1}\bar{1}20]$ direction (Z), and the width of PL (W) were varied.

After the groove formation, to suppress the DPB generation, a specific cubic close-packed structure was exposed on the topmost surface of the substrate by Step-Alignment® treatment, and then a slightly nitrogen doped 5.5 μm-thick SiC layer was epitaxially grown on it.

The distribution of the crystal structures in the epilayer formed by SLE was evaluated using scanning electron microscopy (SEM) combining with electron backscatter diffraction (EBSD). The orientation relationship of each crystal plane of epilayer was determined by inverse pole figures (IPFs) of EBSD. The stacked structure and lattice image of the 3C-SiC/4H-SiC interface were observed using cross-sectional transmission electron microscopy (XTEM). The distribution of carriers in the epilayer was quantified using scanning microwave microscopy (SMM), and the conduction type of the carriers was identified by scanning capacitance microscopy (SCM).

Results and Discussion

First, we focus on one of the SLE grown layers, area-1. In the SEM image shown in Fig. 3 a), the left half of each plateau (on the $[\bar{1}\bar{1}20]$ side) is occupied by a bright region about 75 μm wide, and the remaining right half (on the $[11\bar{2}0]$ side) is occupied by a dark region. The boundary between the bright and dark regions is a straight line parallel to the $[\bar{1}100]$ direction.

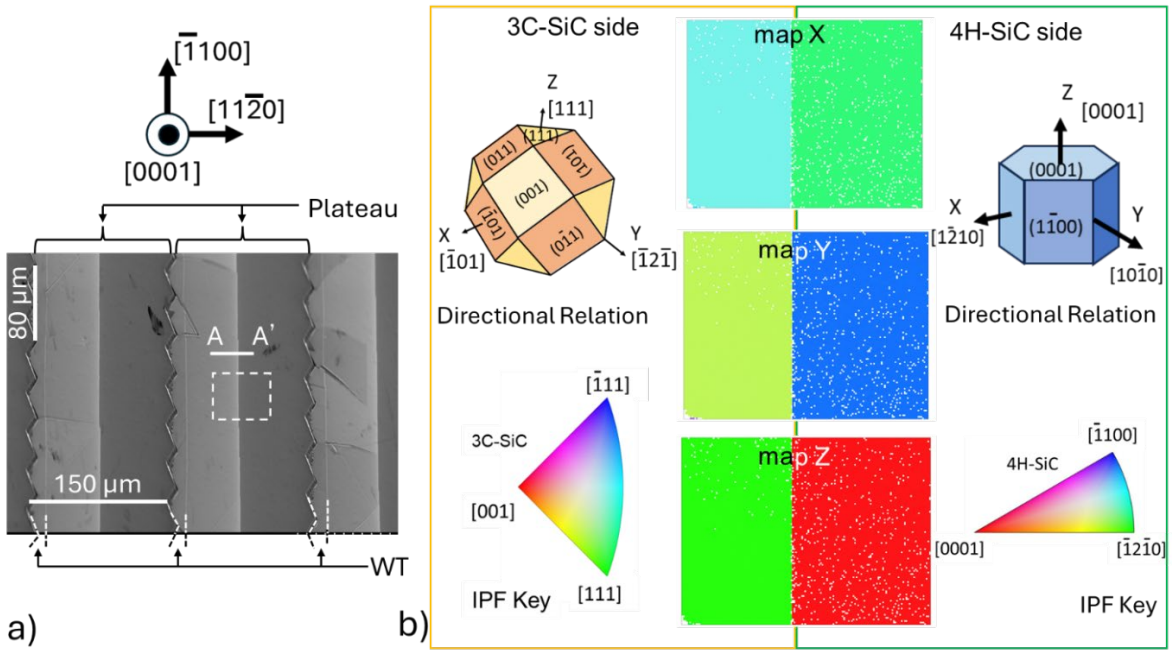

Fig. 3. SEM image and IPF maps in area-1: a) SEM image; b) IPF maps of the region surrounded by the dashed square in fig a).

The IPF maps of the region surrounded by the dashed square in Fig. 3 a), which includes the boundary between the bright and dark regions, are shown in Fig. 3 b). It is obvious that the bright region corresponds to 3C-SiC, and the dark region corresponds to 4H-SiC. The map Z shows that the orientation of the 3C-SiC(111) and 4H-SiC(0001) planes coincide. In addition, the orientation of 3C-SiC($\bar{1}$01) and 4H-SiC(1$\bar{2}$10) planes coincide in map X and the orientation of 3C-SiC($\bar{1}$2$\bar{1}$) and 4H-SiC(10$\bar{1}$0) planes coincide in map Y. It is clear that the 3C-SiC layer corresponding to the bright region in Fig. 3 a) shares the same basal plane with the 4H-SiC layer in the dark region and does not contain DPBs.

In Fig. 3 a), a WT can be found on the plateau adjacent to the downstream side of the groove. The shape of the WT is schematically represented in Fig. 4. When a virtual circle (C_v) with the outer edges of the WT as tangents is overwritten, the diameter of C_v corresponds to w_c. The geometrically calculated w_c is 14.9μm. The 8 μm-wide groove is thought to act as an obstacle to the lateral growth of 4H-SiC toward downstream, maintaining the WT width greater than w_c.

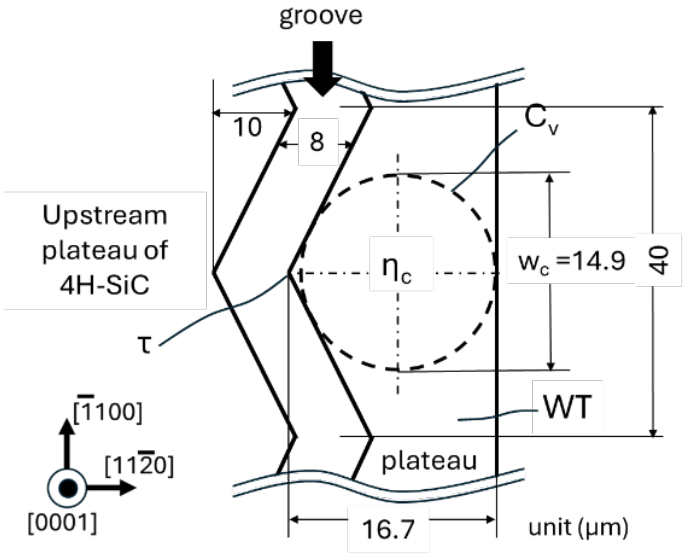

Fig. 4. Schematic plan view of WT in area-1: When a virtual circle (C_v) with the outer edges of the WT as tangents is overwritten, the diameter of C_v corresponds to the critical value for spontaneous nucleation of 3C-SiC (w_c = 14.9μm).

Fig. 5 shows XTEM images of the $(1\bar{1}00)$ cross section along the A-A' line overlayed in Fig. 3 a), which includes the boundary between 3C-SiC and 4H-SiC regions. The global image shown in Fig. 5 a) indicates that the 3C-SiC layer is stacked on the 4H-SiC layer forming an interface (IF_0) parallel to the basal plane. The angle at which the interface intersects the surface of the epitaxial layer corresponds to 4 degrees, the tilt angle of the 4H-SiC substrate. Fig. 5 b), which is a high magnification lattice image, shows that the IF_0 forms an atomically flat plane, and its stacking structure is uniform. As a result, the structure of the SiC epilayer in area-1 is shown schematically in Fig. 5 c), in which the 3C-SiC$(\bar{1}\bar{1}\bar{1})$ C- and 4H-SiC(0001) Si-faces bind each other forming a coherent interface in the basal plane.

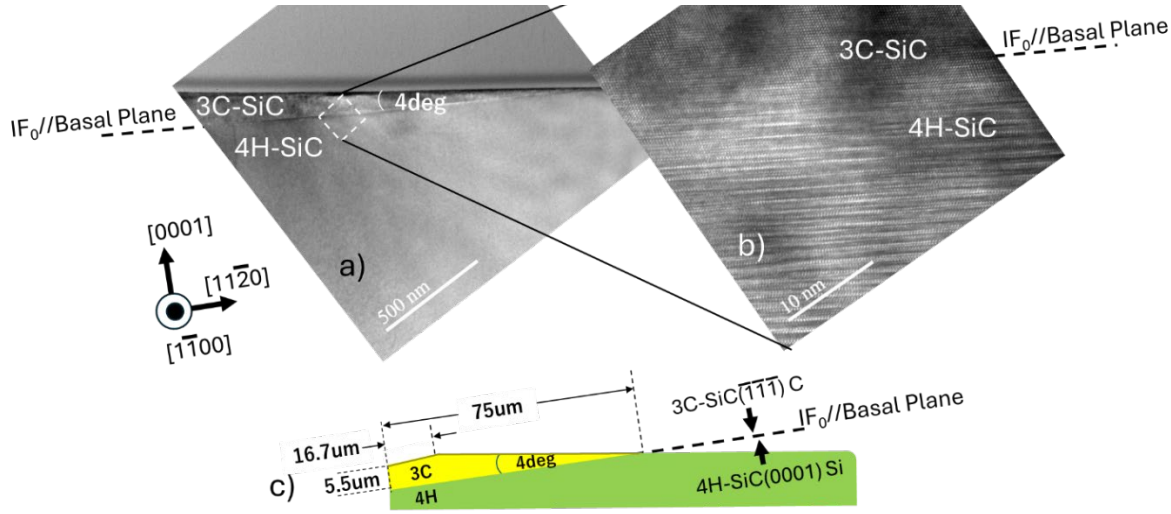

Fig. 5. XTEM images and schematic structure of the SiC epilayer in area-1: a) Global image; b) Lattice image at the 3C-/4H-SiC interface (IF_0); c) Schematic structure of 3C-SiC/4H-SiC stack.

Next, we focus on area-2. In the SEM image of the epilayer surface shown in Fig. 6 a), most of the area on the plateau exhibits a dark contrast (4H-SiC). However, a bright line (L) parallel to the $[\bar{1}100]$ direction can be found at a distance of about 70 μm from the groove edge. The IPF maps in Fig. 6 b), which were observed in the same area as Fig. 6 a), show that single-domain 4H-SiC is exposed in most of the area-2, but the L observed in Fig. 6 a) corresponds to 3C-SiC, whose (111) plane orients in the same direction as that of 4H-SiC(0001) plane.

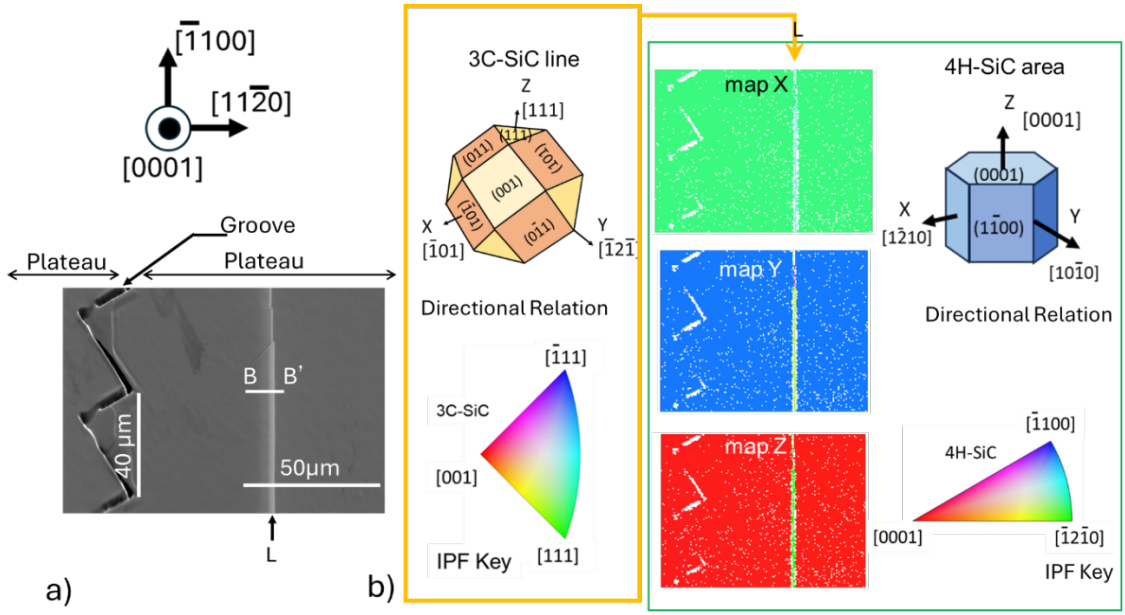

Fig. 6. SEM image and IPF maps in area-2: a) SEM image; b) IPF maps.

Unlike in Fig. 3 a), the WT adjacent to the downstream side of the groove, whose width should exceed 14.9 μm, cannot be found in Fig. 6 a). It is considered that the obstacle to the lateral growth of 4H-SiC toward downstream disappears during the epitaxial growth in area-2. In other words, after the 3C-SiC layer has expanded on the WT, the upstream plateau consists of 4H-SiC grows laterally on the 3C-SiC layer as explained in Fig. 1. Considering the remarkable difference in the shape of the grooves in area-1 and -2, the width of the groove (S) is one of the important factors that define the formation of the multilayer structure and the thickness of the 3C-SiC intermediate layer.

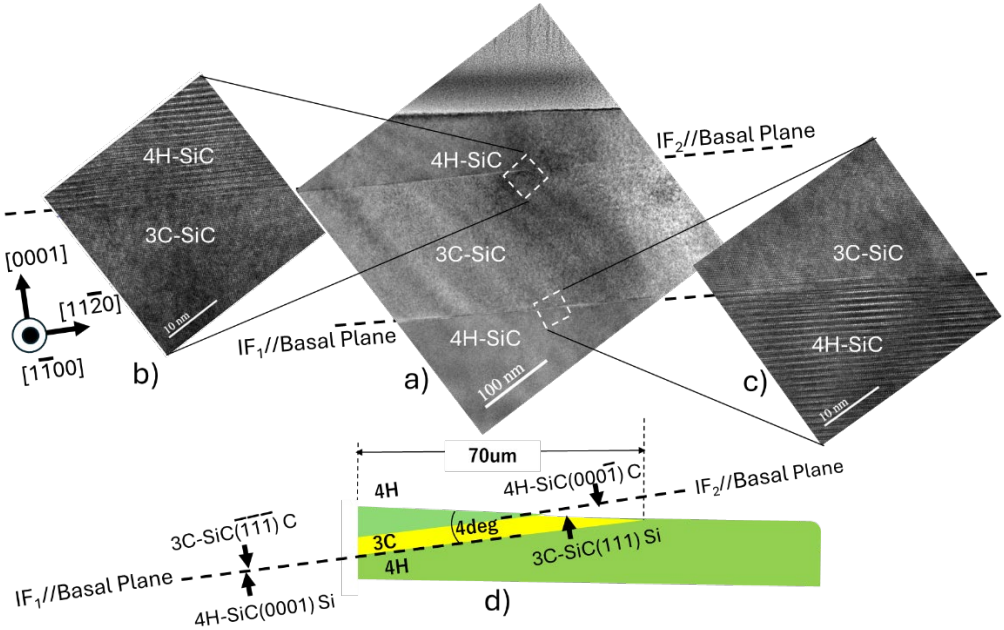

Fig. 7. XTEM images and schematic structure of the SiC epilayer in area-2: a) Global image; b) Lattice image at the interface (IF_2) between the middle 3C-SiC and the top 4H-SiC layers; c) Lattice image at the interface (IF_1) between the bottom 4H-SiC and the middle 3C-SiC layers; d) Schematic structure of 4H/3C/4H-SiC stack.

The XTEM images of the $(1\bar{1}00)$ cross-section along the B-B' line superimposed in Fig. 6 a) is shown in Fig. 7. Two interfaces parallel to the basal plane can be found in the global image of Fig. 7 a). One interface (IF_1) is formed in the deeper part of the epilayer, which is the boundary between the bottom 4H-SiC layer and the middle 3C-SiC layer. The upper interface (IF_2) is the boundary between the middle 3C-SiC layer and the top 4H-SiC layer. Both interfaces are parallel to the basal plane and intersect the surface of each epilayer at an angle of 4 degrees, which is the same as the tilt angle of the substrate. High-magnification lattice image in Fig. 7 b) shows that the IF_2 corresponds to coherent interface, because it shows an atomically flat and uniform stacking sequence. Also the IF_1 is a coherent interface as seen in Fig. 7 c). As schematically shown in Fig. 7 d), the epilayer structure in area-2 consists of a 3C-SiC middle layer sandwiched between 4H-SiC layers, with the 3C-SiC$(\bar{1}\bar{1}\bar{1})$ C-face and 4H-SiC(0001) Si-face facing each other at the IF_1 and the 4H-SiC$(000\bar{1})$ C-face and 3C-SiC(111) Si-face each other at IF_2.

It is known that the coherent interface where the 3C-SiC$(\bar{1}\bar{1}\bar{1})$ C-face and 4H-SiC(0001) Si-face are bound each other forms 2DHG with the sheet carrier density about 3.5×10^{12} cm^{-2} [5], and the coherent interface where the 4H-SiC$(000\bar{1})$ C-face and 3C-SiC(111) Si-face are bound forms high electron mobility 2DEG with the sheet carrier density above 10^{13} cm^{-2} [1, 8, 9]. These are considered to be caused mainly by positive or negative fixed charges induced by spontaneous polarization at the heterointerfaces, which is dependent on the degree of hexagonality in SiC polytypes [10]. Additionally, thanks to the large conduction band offset (0.99 eV, [11]), it is suggested that free electron accumulation in 2DEG can be effectively induced in the 3C-SiC layer [8]. Based on the above findings, it is considered that only 2DHG exists in the cross-section of area-1 (including only IF_0), while 2DEG and 2DHG coexist in the cross section of area-2 (including IF_1 and IF_2).

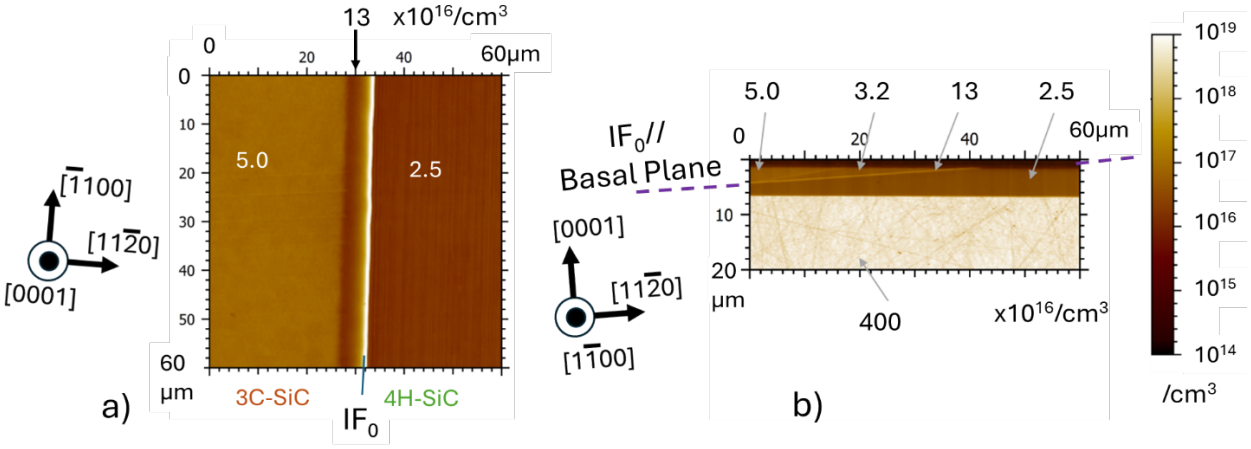

Fig. 8. SMM images observed in area-1: a) Plane image; b) Cross-sectional image.

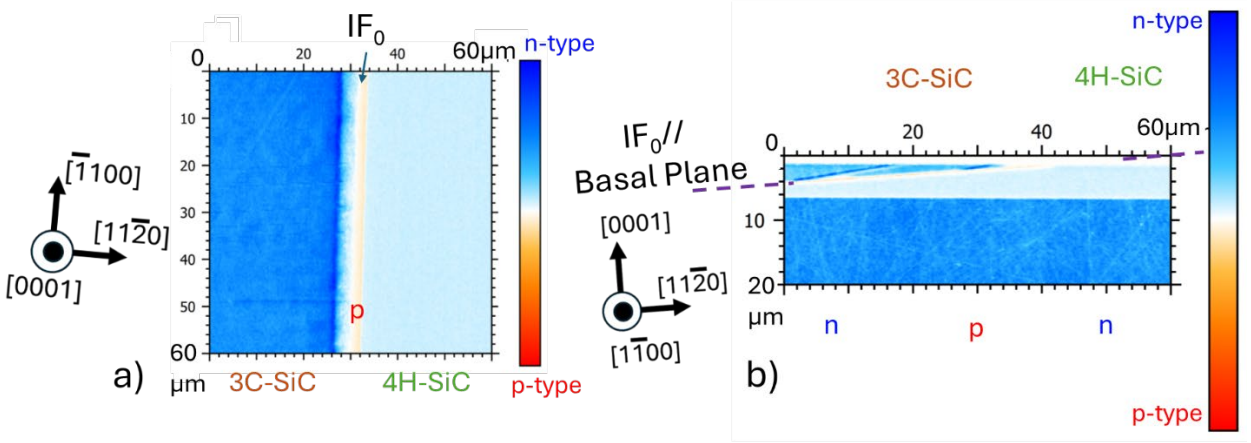

Fig. 9. SCM images observed in area-1: a) Plane image; b) Cross-sectional image.

Fig. 8 shows the SMM images observed in area-1. The observation was carried out so as to include the IF_0. The intensity of the SMM signal depends on the carrier density, and darker and brighter colors indicates lower and higher carrier density, respectively. It should be noted that, due to the principles of SMM, the measured value is the density per volume, and the sheet carrier density cannot be obtained. As shown in the plane image shown in Fig. 8 a) and the cross-sectional image in Fig. 8 b), a carrier density of 2.5×10^{16} cm^{-3} is found in the layer corresponding to 4H-SiC, and 3.2×10^{16} $cm^{-3} \sim 5.0 \times 10^{16}$ cm^{-3} in the layer corresponding to 3C-SiC. The difference in carrier density between the 3C-SiC and 4H-SiC layers may be influenced by the differences in activation rate or compensation of doped nitrogen. Notably, a carrier density of 1.3×10^{17} cm^{-3} is observed along the line corresponding to IF_0. To identify the conduction type of the carriers observed above, the SCM images observed simultaneously with the SMM are shown in Fig. 9. Here, polarity and intensity of SCM signal are attributed to conduction type (p- or n-type) and carrier density, respectively. Figs a) and b) show the planar and cross-sectional images of the SCM, respectively. Those clearly show that the conduction type of the 3C-SiC and 4H-SiC layers is n-type, while it is p-type on the line corresponding to IF_0. This means that 2DHG is generated exactly at the boundary between 3C-SiC$(\bar{1}\bar{1}\bar{1})$ and 4H-SiC(0001).

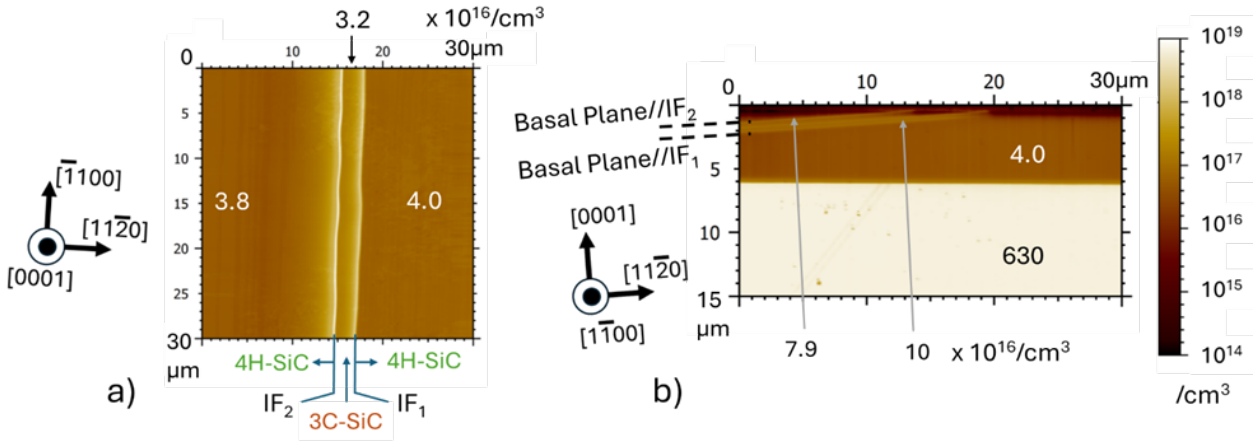

Fig. 10. SMM images observed in area-2: a) Plane image; b) Cross-sectional image.

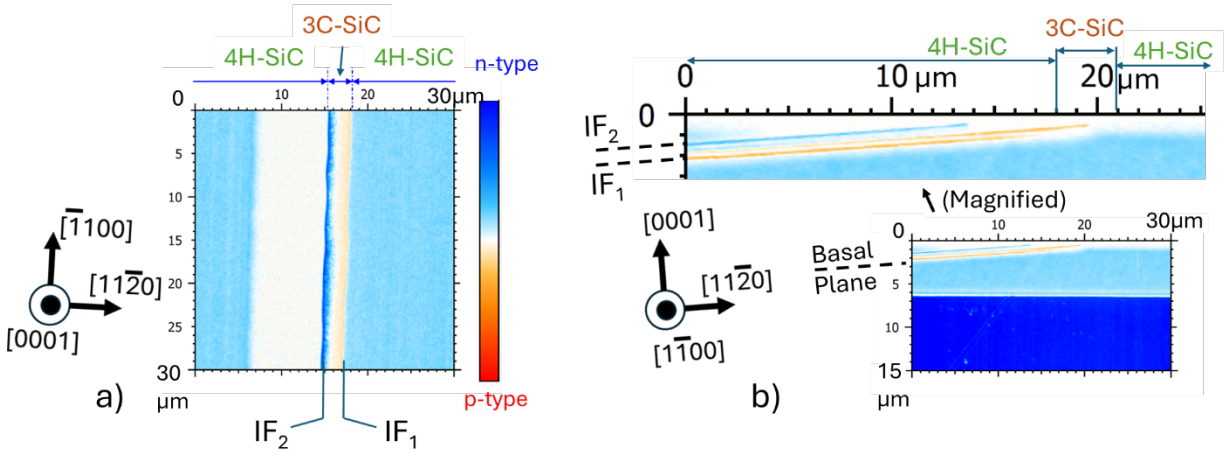

Fig. 11. SCM images observed in area-2: a) Plane image; b) Cross-sectional image.

The SMM images observed in area-2 are shown in Fig. 10. In the surface image (Fig.10 a), a couple of bright lines (high carrier density regions) can be seen along the IF_1 and IF_2 intercepts on the surface. On the other hand, on the top 4H-SiC epilayer (x = 0 ~ 15 μm) and on the bottom 4H-SiC epilayer (x = 18 ~ 30 μm), lower density regions (indicated by brown) can be seen, and carrier density is determined to be 3.8×10^{16} cm^{-3} and 4.0×10^{16} cm^{-3}, respectively. At the cross-sectional image (Fig. 10 b), carrier-depleted regions can be seen near the surface. Additionally, two higher carrier density regions (indicated by light yellow bands) can be identified at IF_1 and IF_2, and they reach surface along the basal plane through the depleted region. The SCM image observed in the same area is shown in Fig. 11. In particular, the darkest color corresponds to the highest carrier density (7.9×10^{16} cm^{-3} for IF_2 1.0×10^{17} cm^{-3} for IF_1). In the SCM surface image (Fig. 11a), the n-type region (shown in light blue or blue) and the p-type region (shown in orange) are clearly visible. The prominent n- and p-type regions correspond to the locations where IF_2 and IF_1 are exposed on the surface, respectively. Fig. 11 b) shows the SCM cross-sectional image. The light blue and orange lines parallel to the basal plane are thought to correspond to the 2DEG formed along IF_2 and the 2DHG formed along IF_1, respectively. Considering the spatial resolution of the SCM, the actual local carrier density of the 2DEG and 2DHG is likely to be much higher than 10^{17} cm^{-3}. In this way, we have successfully demonstrated that simultaneous formation of 2DEG and 2DHG can be realized on a 4H-SiC(0001) Si-face.

Conclusion

To generate 2DEG and 2DHG in the SiC polytype heteroepitaxial layers at will, multilayer epitaxial growth of 3C-SiC and 4H-SiC was demonstrated. Formation of a groove with a vertex in the $[\bar{1}\bar{1}20]$ direction was found to act as an efficient blocker against the step-controlled epitaxy of 4H-SiC, and to obtain single-nucleus 3C-SiC on the atomically flat wide terrace at predetermined location. This method also enables us to obtain a 4H-SiC/3C-SiC/4H-SiC multilayer structure by conducting the step-controlled epitaxy of alternative 4H-SiC, which prevents continuous nucleation on the 3C-SiC layer obtained on 4H-SiC. 2DHG is formed at the coherent interface between the 3C-SiC$(\bar{1}\bar{1}\bar{1})$ C- and the 4H-SiC(0001) Si-faces whilst 2DEG is formed at the coherent interface between the 3C-SiC(111) Si- and the 4H-SiC$(000\bar{1})$ C-faces. In this way, we have demonstrated a technology for forming 3C-SiC/4H-SiC multilayer structures at specific locations by SLE method. This technology opens the way to applications such as high-frequency devices using 2DEG and 2DHG as well as CMOS integrated circuits with resistance to high voltage, higher temperatures and strong radiation environments.

Acknowledgement

The authors would like to express their sincere gratitude to Ceramic Forum Co., Ltd. for providing patterned SiC wafers and performing epitaxial growth on them, and to Dry Chemicals Co., Ltd. for performing the Step-Alignment® treatment to obtain single-domain SiC epitaxial layers.

References

[1] H. Sazawa, H.Yamaguchi, Appl. Phys. Lett. 120, 212102 (2022)

[2] H. Sazawa, A. Nakajima, S. Kuboya, H. Umezawa, T. Kato, Y. Tanaka, Appl. Phys. Lett. 124, 120601 (2024)

[3] H. Nagasawa, Y. Cho, M. Abe, T.Tanno, M. Musya, M. Sakuraba, Y. Sato, S. Sato, Solid State Phenomena 362, 33-40 (2024)

[4] H. Nagasawa, U.S. Patent 11,862,460. (2021)

[5] M.V.S. Chandrashekhar, C.I. Thomas, J. Lu, M.G. Spencer, Appl. Phys. Lett. 90, 173509 (2007)

[6] M.V.S. Chandrashekhar, J. J. Parks, D. C. Ralph, M. G. Spencer, Appl. Phys. Lett. 94, 162115 (2009)

[7] D. J. Larkin and J. A. Powell, U.S. Patent 5,363,800. (1991)

[8] M. V. S. Chandrashekhar, C. I. Thomas, J. Lu, M. G. Spencer, Appl. Phys. Lett. 91, 033503 (2007)

[9] V. M. Polyakova, F. Schwierz, J. Appl. Phys. 98, 023709 (2005)

[10] A. Qteish, R. J. Needs, V. Heine, Comput. Mater. Sci. 2, 389 (1994)

[11] P. Käckell, B. Wenzien, F. Bechstedt, Phys. Rev. B, 50, 10761 (1994)